Quasibound states in the continuum for flexural waves

Shengming Sun [1], Yabin Jin [2], and Dani Torrent [1,*]

[1] *GROC, UJI, Institut de Noves Tecnologies de la Imatge (INIT), Universitat Jaume I, 12071 Castelló, Spain*

[2] *Institute of Computational Mechanics × AI & College of Intelligent Robotics and Advanced Manufacturing, Fudan University, 200433 Shanghai, China*

(Received 13 October 2025; revised 28 January 2026; accepted 27 February 2026; published 15 April 2026)

Bound states in the continuum (BICs) and their quasibound counterparts (QBICs) have emerged as powerful tools to engineer sharp resonances and extreme field confinement in wave systems. Here, we investigate the formation and tunability of BICs and QBICs for flexural waves in thin elastic plates decorated with a one-dimensional array of pointlike resonators. By designing a diatomic unit cell and varying the relative angle of the two resonators, we achieve precise control over the coupling between the guided modes of the plate and the radiation continuum. This simple geometric tuning enables the transition from a symmetry-protected BIC at the center of the Brillouin zone to a family of high-Q QBICs at finite Bloch wave vectors. We develop an analytical multiple-scattering model to compute the transmission and reflection coefficients of a plane flexural wave interacting with the array, and we demonstrate that the resulting resonances manifest as angle-dependent Fano line shapes in the scattering spectra. Furthermore, by employing a lumped-element description of the resonators, we propose a feasible physical realization of the system and validate our theoretical predictions against full finite element simulations, obtaining excellent quantitative agreement. Our results provide both a fundamental understanding and a practical route to engineer ultranarrow resonances and elastic metasurfaces with tailored dispersion, paving the way for advanced control of flexural waves in thin plates.

DOI: 10.1103/28wk-3ss7

I. INTRODUCTION

Bound states in the continuum (BICs) are localized eigenmodes that exist spectrally within the continuum of radiating states but remain perfectly confined due to symmetry constraints or destructive interference [1]. Originally conceived in quantum mechanics [2–4], the concept has since been generalized to photonics [5–8], acoustics, and elastodynamics, where it enables extreme field confinement, ultrahigh quality factors and strong wave-matter interactions in open systems [9–18].

In realistic structures, ideal BICs are usually perturbed by slight symmetry breaking or structural imperfections, leading to quasi-BICs (QBICs)—long-lived resonances that weakly couple to the continuum. These modes preserve many of the advantages of true BICs while being accessible from the far field. Their radiative coupling strength and quality factor can be tuned by adjusting the degree of symmetry breaking, modifying the unit cell geometry, or varying the incidence angle of an external excitation. As a result, QBICs manifest as sharp, asymmetric Fano resonances in scattering spectra [9,19–23].

Recent developments in photonic and phononic platforms have expanded the range of available BIC phenomena, including the merging of accidental and symmetry-protected BICs [10,24–26], hybridization of multiple BIC channels [19,27], and robust BICs in metasurfaces and polaritonic systems [20]. These studies demonstrate that BIC physics is not restricted to electromagnetic waves but extends naturally to acoustic and elastic systems.

In the field of flexural waves in thin plates, arrays of pointlike resonators offer a powerful route to engineer band structures and localized modes [28]. Finite clusters of resonators can sustain extremely high-Q localized modes that converge to BICs in the infinite-array limit, while periodic structures enable the design of edge and interface states with robust transport properties [29,30]. Experimental demonstrations of acoustic BICs further underscore the versatility of this concept beyond optics [31].

In elastic and acoustic wave systems, linear periodic arrays have long been known to support guided and leaky modes, often referred to as Rayleigh-Bloch waves. Early studies considered resonance and wave trapping effects in periodic structures and wake-induced oscillations [13,14]. More recently, linear chains of resonant pillars on elastic or semi-infinite substrates have been investigated, revealing rich dispersive behavior and strong wave-resonator interactions [32].

In parallel, a growing body of work has focused on the complex dispersion relations of Rayleigh-Bloch waves in open periodic systems [33–35]. Although based on scalar wave equations, these studies exhibit strong qualitative similarities with flexural-wave systems, including the emergence of leaky modes, avoided crossings, and sharp resonances associated with radiation losses.

*Contact author: dtorrent@uji.es

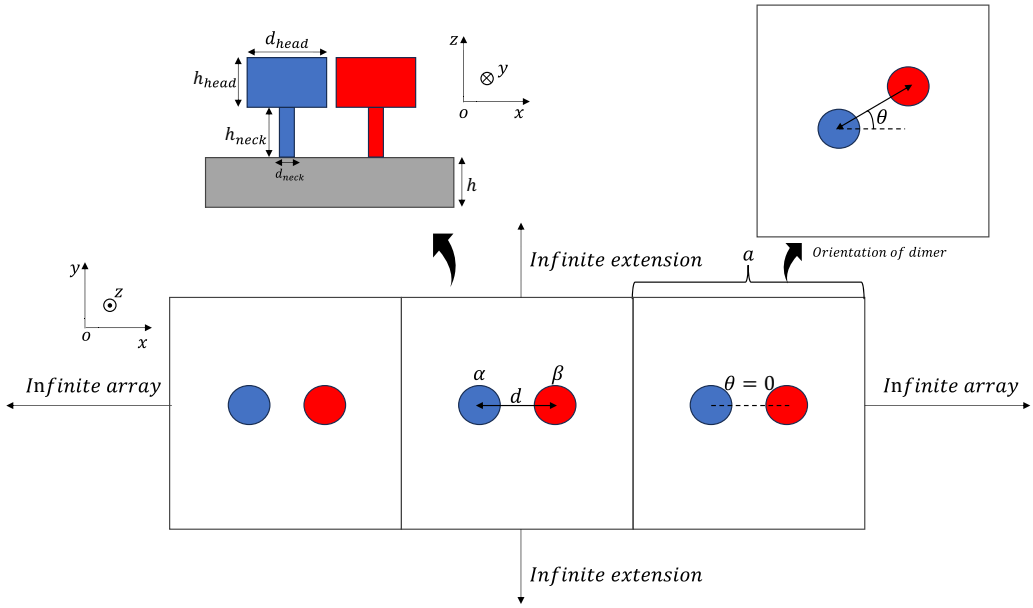

FIG. 1. Schematic of the system under study: an infinite linear periodic array of resonant head-neck attachments placed on a thin elastic plate. The array is periodic along the x direction with lattice constant a. Each unit cell contains two resonators separated by a distance d, forming a dimerized geometry, which eventually can be rotated an angle θ to break the symmetry.

In this work, we extend these ideas to flexural waves in thin elastic plates, using a multiple-scattering framework based on Kirchhoff-Love plate theory, and demonstrate the existence of symmetry-protected bound states in the continuum and tunable quasi-BICs in a linear array of resonant attachments.

We explore BIC and QBIC formation in a linear array of pointlike resonators on a thin elastic plate, where each unit cell consists of two resonators with tunable relative positions. This simple dimerized geometry folds the Brillouin zone and supports a symmetry-protected BIC at the Γ point, while also enabling a tunable quasi-BIC band across the Brillouin zone. By varying the relative displacement between the two resonators, we continuously control the radiative leakage and quality factor of the resonance. Furthermore, by changing the angle of incidence of an incoming plane wave, we selectively excite QBICs with different in-plane wave vectors, revealing a family of angle-dependent Fano resonances associated with the QBIC dispersion.

Our results demonstrate how a minimal one-dimensional resonant structure can host both symmetry-protected and tunable quasi-BICs for flexural waves. Beyond their fundamental interest, such modes could enable narrow band filters, enhanced elastic sensing platforms, and nonlinear wave manipulation in mechanical metasurfaces.

II. THEORETICAL FORMULATION

The schematic representation of the system is shown in Fig. 1. We consider a linear array of pointlike scatterers periodically distributed along the x axis and attached to a thin elastic plate of thickness h. The unit cell, of length a, consists of two scatterers separated by a relative displacement vector $\boldsymbol{d}$, initially aligned with the x axis but which can be rotated by an angle θ_0. As will be shown later, this rotation acts as a control parameter for the system's resonant response.

The periodicity of the structure allows to label eigenmodes as a function of the Bloch wave number k_x along the x direction. When the rotation angle between the scatterers θ_0 is zero, the two scatterers form a symmetric unit cell with respect to the y axis which, at the Γ point of the Brillouin zone (corresponding to $k_x = 0$), supports a set of eigenmodes with well-defined parity. These modes are obviously above the so-called radiation continuum so that, in principle, they should be leaky. However, modes with odd symmetry cannot be coupled to this continuum, consequently they remain trapped at the array of scatters. These modes are called symmetry-protected bound states in the continuum (BICs). The only way of getting this family of modes with point scatterers is by placing more than one scatterer per unit cell, as can be easily deduced from the multiple scattering formulation of the problem. Breaking the symmetry of the unit cell allows to control the quality factor of these perfectly trapped modes, and we will do it in two ways in this work: by rotating the relative displacement vector $\boldsymbol{d}$ or by changing the Bloch wave number k_x.

Pointlike scatterers are modeled as spring-mass attachments characterized by its mass m_0 and spring constant κ_0, which additionally defines its resonant frequency ω_r. The physical implementation of the pointlike resonators described in the analytical model can be realized using a head-neck (or mass-spring) configuration, as illustrated schematically in Fig. 1. This approach, introduced in Ref. [36], provides an effective subwavelength resonator whose mechanical response can be accurately captured using a lumped-parameter description. In this system, the enlarged "head" behaves as a concentrated mass, while the slender "neck" acts as an elastic spring that connects the resonator to the host plate.

Under the assumption that the local deformation is dominated by axial compression and extension of the neck, the

lumped mass (m_0) and stiffness (κ_0) of the resonator are given by

$$m_0 = \frac{\pi \rho_{\text{head}} d_{\text{head}}^2 h_{\text{head}}}{4} + \frac{\pi \rho_{\text{neck}} d_{\text{neck}}^2 h_{\text{neck}}}{4}, \tag{1}$$

$$\kappa_0 = \frac{\pi E_{\text{neck}} d_{\text{neck}}^2}{4 h_{\text{head}}}, \tag{2}$$

where ρ_X, d_X, h_X, and E_X, with $X =$ head, neck, denote the material density, diameter, height, and Young's modulus of each component. This head-neck system therefore acts as a localized flexural resonator with a well-defined fundamental resonance.

To incorporate these elements into the multiple-scattering framework explained below, it is useful to express the resonator's properties using two dimensionless parameters: the normalized resonance frequency Ω_r and the normalized resonator mass γ, defined as

$$\Omega_r = a\sqrt{\frac{\kappa_0}{m_0}\frac{\rho h}{D}}, \tag{3}$$

$$\gamma = \frac{m_0}{\rho a^2 h}, \tag{4}$$

where a denotes the lattice constant of the array of resonators while ρ, h, and D are the density, thickness, and bending rigidity of the plate, this last parameter being related with the Young modulus E and Poisson's ratio ν by

$$D = \frac{E h^3}{12(1-\nu)}. \tag{5}$$

The theoretical framework builds upon our earlier work on the multiple scattering of pointlike resonators attached to thin elastic plates [28,37]. There, an analytical formalism was established within the Kirchhoff-Love plate theory [38], in which the plate is characterized by its density ρ, rigidity D, and thickness h. This formalism yields the total scattered field for arbitrary resonator configurations. Detailed derivations of the scattering coefficients and the multiple-scattering equations can be found in those references and are not repeated here. For the present linear periodic array, the approach provides closed-form expressions for the transmission and reflection coefficients of an incident plane wave. In particular, we focus on the zeroth-order transmitted and reflected modes, whose amplitudes are directly related to the total scattered field generated by the array:

$$\begin{Bmatrix} t_0 - 1 \\ r_0 \end{Bmatrix} = \frac{iG_0}{k \sin\theta_0} \sum_{\beta=1}^{N} B_\beta \times \begin{Bmatrix} e^{-i\mathbf{k}_0^+ \cdot \mathbf{R}_\beta} \\ e^{-i\mathbf{k}_0^- \cdot \mathbf{R}_\beta} \end{Bmatrix}, \tag{6}$$

where B_β represents the scattering coefficient of the β scatterer within the unit cell, $G_0 = i/8k^2$ is the Green's function for flexural waves at the origin of coordinates and $\boldsymbol{k}_0$ is the wave vector of the incident field arriving to the array of scatterers, which forms a θ_0 angle with the x axis and has a modulus k related with the frequency ω by means of the plate dispersion relation

$$\omega = \sqrt{\frac{D}{\rho h}} k^2. \tag{7}$$

The above dispersion relation can be expressed in a more compact form by defining the normalized frequency Ω as

$$\Omega^2 = \omega^2 \frac{\rho a^2 h}{D}, \tag{8}$$

thus we see that

$$\Omega a = k^2 a^2. \tag{9}$$

In the absence of incident field the B_β coefficients are the solutions of a homogeneous system of equations of the form

$$\begin{bmatrix} t_\alpha^{-1} - \chi_{\alpha\alpha} & -\chi_{\alpha\beta} \\ -\chi_{\beta\alpha} & t_\beta^{-1} - \chi_{\alpha\alpha} \end{bmatrix} \cdot \begin{bmatrix} B_\alpha \\ B_\beta \end{bmatrix} = \begin{bmatrix} 0 \\ 0 \end{bmatrix}, \tag{10}$$

with

$$t_\alpha = D\gamma \frac{\Omega^2}{1 - \Omega^2/\Omega_r^2} \tag{11}$$

being the resonant impedance of the pointlike scatterer and the quantities

$$\chi_{\alpha\beta} = \frac{1}{4D\Omega} \sum_n e^{-i2n\pi x_{\alpha\beta}/a} \left[\frac{e^{-\zeta^- |y_{\alpha\beta}|}}{\zeta^-} - \frac{e^{-\zeta^+ |y_{\alpha\beta}|}}{\zeta^+} \right] \tag{12}$$

with

$$\zeta^\pm = \sqrt{\left(K_x + \frac{2n\pi}{a}\right)^2 \pm \omega\sqrt{\frac{\rho h}{D}}}, \tag{13}$$

represents the multiple scattering coupling.

The above system of equations has nontrivial solutions only for those frequencies for which the determinant of the 2×2 multiple scattering matrix is zero. These conditions usually can be satisfied for complex frequencies only, and correspond to the eigenmodes of the system. However, under certain conditions, real frequencies exist that satisfy these equations, whose location in the Brillouin zone where they are located defines a guided wave or a bound state in the continuum (BIC). Small perturbations of the latter modes, which correspond to modes with a high quality factor but still complex in frequency, are called quasibound states in the continuum or QBICS.

When an external plane wave arrives to this linear array of scatterers the system of equations is no longer homogeneous and reads

$$\begin{bmatrix} t_\alpha^{-1} - \chi_{\alpha\alpha} & -\chi_{\alpha\beta} \\ -\chi_{\beta\alpha} & t_\beta^{-1} - \chi_{\alpha\alpha} \end{bmatrix} \cdot \begin{bmatrix} B_\alpha \\ B_\beta \end{bmatrix} = \begin{bmatrix} e^{i\mathbf{k}\cdot\mathbf{R}_\alpha} \\ e^{i\mathbf{k}\cdot\mathbf{R}_\beta} \end{bmatrix}, \tag{14}$$

whose solutions B_β are given by

$$B_\alpha = \frac{\left(t_\beta^{-1} - \chi_{\alpha\alpha}\right) e^{i\mathbf{k}\mathbf{R}_\alpha} + \chi_{\alpha\beta} e^{i\mathbf{k}\mathbf{R}_\beta}}{\left(t_\alpha^{-1} - \chi_{\alpha\alpha}\right)\left(t_\beta^{-1} - \chi_{\alpha\alpha}\right) - \chi_{\alpha\beta}\chi_{\beta\alpha}}, \tag{15}$$

$$B_\beta = \frac{\chi_{\beta\alpha} e^{i\mathbf{k}\mathbf{R}_\alpha} + \left(t_\alpha^{-1} - \chi_{\alpha\alpha}\right) e^{i\mathbf{k}\mathbf{R}_\beta}}{\left(t_\alpha^{-1} - \chi_{\alpha\alpha}\right)\left(t_\beta^{-1} - \chi_{\alpha\alpha}\right) - \chi_{\alpha\beta}\chi_{\beta\alpha}}. \tag{16}$$

In the following sections we will analyze the eigenmodes of the structure proposed in Fig. 1 and the transmission properties of plane waves at different incidence angles to show the existence of BICs and QBICs as well as their response to far-field excitations. We will use scatterers with a reduced mass $\gamma = 0.09$ and resonant frequency $\Omega_r a = 13$,

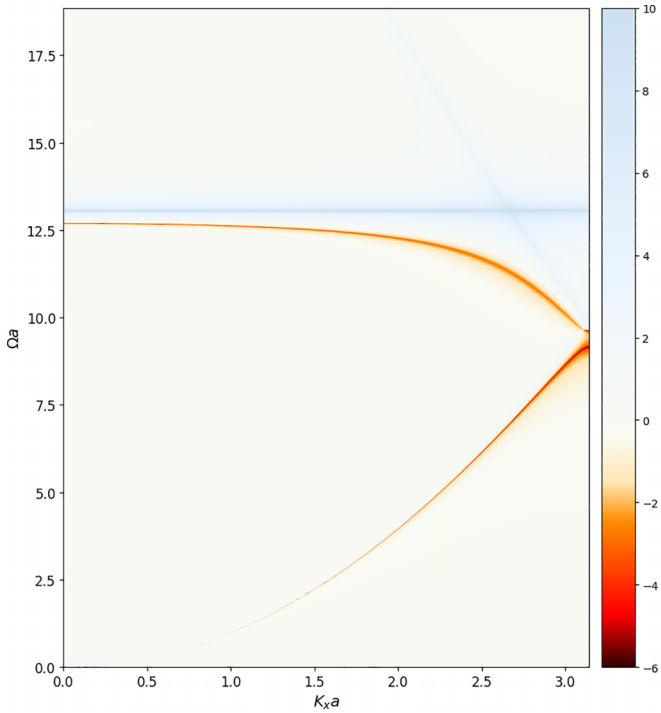

FIG. 2. Color map of $\log_{10}|\det M|$ as a function of the reduced frequency Ωa and Bloch wave number $k_x a$. Small values of the determinant (red) indicate resonant conditions. The nearly horizontal feature near the scatterer's resonance frequency corresponds to the intrinsic local resonance of the scatterers and does not represent a propagating Bloch mode. The curved red band corresponds to a quasibound state in the continuum (QBIC), while a symmetry-protected BIC occurs at the Γ point ($k_x = 0$).

whose physical implementation will be discussed in Sec. V. Also, we will assume that the plate has a thickness $h = 0.2a$ and it is made of aluminium. The scatterers are initially located at $x_\alpha = -3/16a$ and $x_\beta = 3/16a$, although they will be rotated within the unit cell to break the symmetry.

III. BICS AND QBICS AT THE Γ POINT

Figure 2 shows a 2D color map of the logarithm of the determinant of the multiple scattering matrix defined in Eq. (10) as a function of the reduced frequency Ωa and the Bloch wave number $k_x a$. The closer the parameter to $-\infty$, the better the quality factor of the mode. It can be shown that below the radiation cone $\Omega a = (ka)^2$ the determinant of the matrix is strictly zero, however numerical precision was not enough to find a better value for this map (better algorithms show exactly where the zeros are, but this is not the objective of the present work). We see also how outside the radiation cone some nearly flat bands with a strong red color exist. As will be seen later, these bands does not correspond to a zero of the determinant but to a very small value. Finally, it cannot be clearly seen in the color map, but at $k_x = 0$ a set of modes with an infinite lifetime (zero determinant) appear. These modes are symmetry protected BIC and their existence and perturbation will be discussed in this section. We can see also some blue lines crossing the map, but it has to be pointed out that these lines are only high values of the determinant and do not

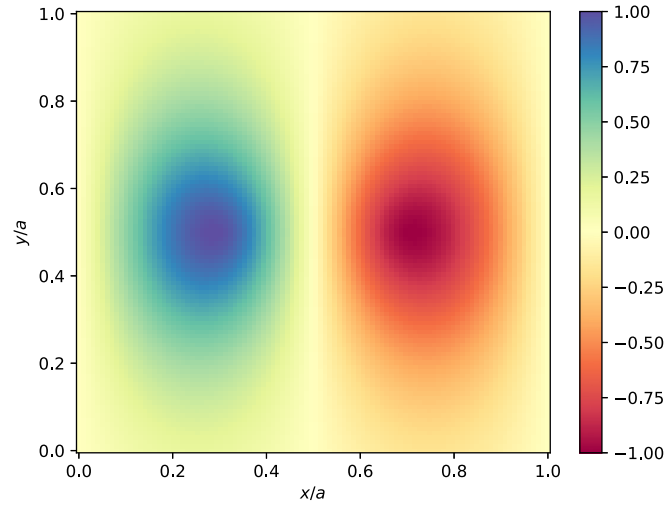

FIG. 3. Out-of-plane displacement field associated with the symmetry-protected BIC at the Γ point. The field exhibits odd parity with respect to the center of the unit cell, leading to destructive interference of radiated waves and complete suppression of radiation despite lying within the continuum.

correspond to eigenmodes of the system. More specifically, we can see a blue line defining the radiation cone $\Omega a = (ka)^2$ and a horizontal line corresponding to the scatterer's resonant frequency $\Omega_r a\#$.

As was explained before, in general, Eq. (10) has solutions only for complex frequencies, reflecting the leaky nature of resonances in open systems. Linear arrays of scatterers can host purely real solutions, but only below the so-called radiation cone, corresponding to regions of the Brillouin zone where no propagating wave can be emitted along the y direction. In contrast, at special symmetry points above the radiation cone, the mode symmetry may forbid coupling to outgoing waves. This occurs at the Γ point, where $k_x = 0$ and the system is mirror-symmetric with respect to the y axis. As a result, the eigenmodes possess definite parity in x, and Eq. (10) reduces to

$$B_\alpha \pm B_\beta = 0. \tag{17}$$

Odd-parity modes cannot couple to plane waves radiating away from the array, and are therefore perfectly trapped despite lying within the continuum—a manifestation of symmetry-protected BICs. Figure 3 illustrates such an eigenmode ocurring at $\Omega a = 12.7$. The symmetry of the mode is odd, thus it could not be coupled with the $n = 0$ grating mode (the fundamental one), however it will be coupled with the $n = \pm 1$ modes, with propagating wave number along y given by

$$k_y = \sqrt{k^2 - 4n^2\pi^2/a^2}, \tag{18}$$

however, for the frequencies at which this state appears, k_y is complex, what means that the field is evanescent and the mode remains trapped on the line of scatterers.

Since BIC modes are completely decoupled from the radiation continuum, they cannot be excited from the far field. While this isolation can be advantageous, in many cases it is desirable to excite high-Q modes externally. Because

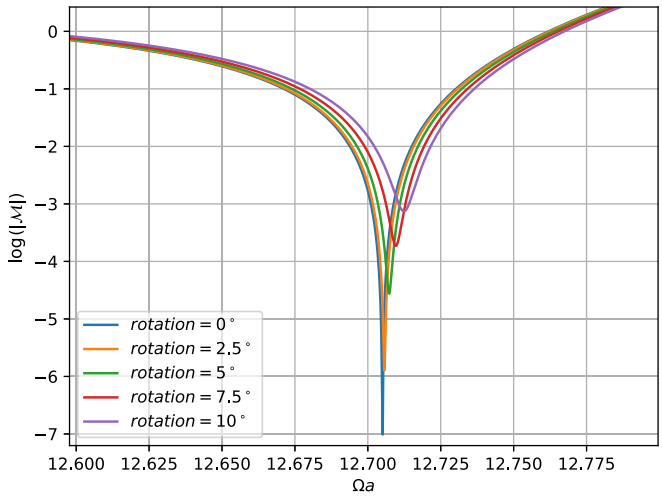

FIG. 4. Logarithm of the determinant of the multiple scattering matrix as a function of frequency for different rotation angles of the resonators within the unit cell.

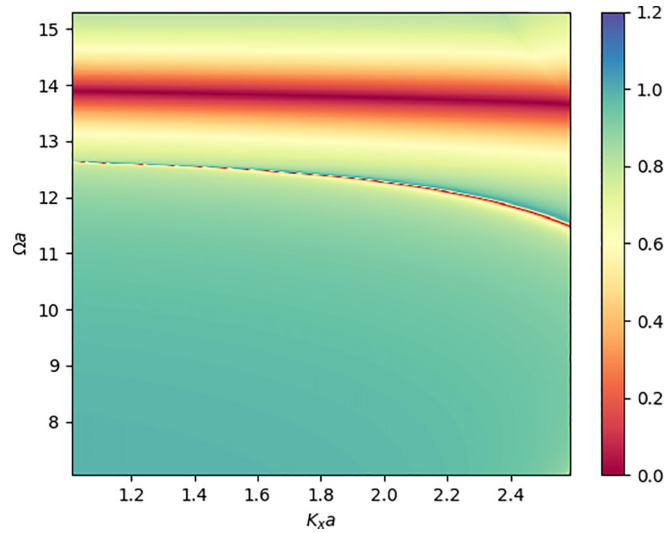

FIG. 6. Transmission coefficient as a function of the reduced frequency Ωa and wave number $k_x a$.

confinement arises from symmetry, small perturbations of the unit-cell geometry transform BICs into QBICs with finite but still high quality factors. Figure 4 shows the logarithm of the determinant of the multiple scattering matrix as a function of frequency for different rotation angles of the dimer vector $\boldsymbol{d}$, and it can be seen how this rotation tunes the quality factor without shifting the resonance frequency. As shown in Ref. [39], the closer the determinant approaches zero, the higher the quality factor.

Having finite quality factors, QBICS can be excited and interrogated from the far field. Figure 5 shows the transmission coefficient of the infinite grating at normal incidence for the different rotation angles of the scatterers. As we see, there is a direct correspondence with the depth and width of the determinant of the matrix shown before and the width of the Fano-like resonance illustrated in the transmission coefficient, while the frequency is nearly invariant. We see also how when the scatterers are rotated 0° there is no interaction with the wave and the mode. This shows how this mechanism can be used to tune the quality factor of the trapped mode with just a relative rotation of the scatterers within the unit cell.

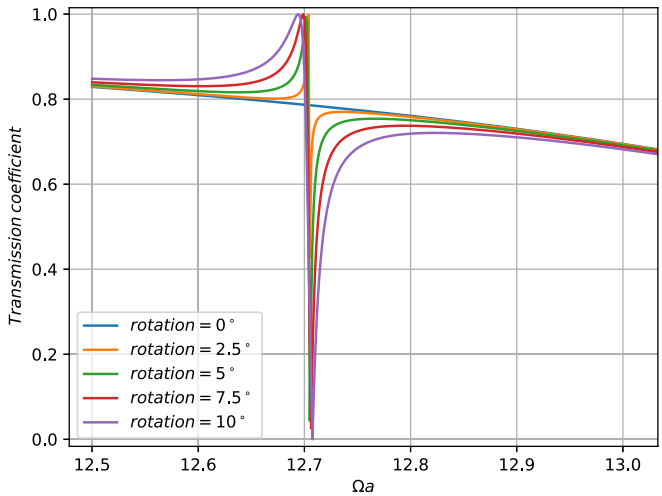

FIG. 5. Transmission coefficient as a function of frequency at normal incidence for different rotation angles of the scatterers in the unit cell.

IV. QBICS ALONG THE BRILLOUIN ZONE

The dispersion diagram in Fig. 2 maps the determinant of the secular matrix M as a function of frequency and the Bloch wave vector along x. True zeros of the determinant occur only below the radiation cone, but near-zero values persist above it. This effect is analogous to that discussed at the Γ point: symmetry breaking determines the quality factor. In this case, the breaking arises from finite Bloch momentum along x, which lifts the mirror symmetry of the wave equation and removes well-defined parity.

As a consequence, QBICs can now couple to external fields, but their excitation requires matching the x component of the wave vector of the incident wave with that of the Bloch mode. Figure 6 shows the transmission coefficient as a function of frequency and $k_x a$. The flat band corresponds to the resonator frequency, while the curved band underneath is the QBIC dispersion, following perfectly the dispersion relation.

A more detailed picture of what happens in the transmission properties of the array can be seen in Fig. 7, where the Fano-like resonance is again shown for $k_x a = 1.5$ and $k_x a = 2.4$. In this occasion, the tuning mechanism for the resonance is the k_x vector, since we can see how the smaller $k_x a$ the better the quality factor of the resonance, reaching the perfectly trapped mode or BIC at $k_x = 0$ or Γ point.

V. FINITE ELEMENT SIMULATIONS

Full-wave numerical simulations were performed using the finite element method (FEM), as implemented in the *Solid Mechanics* module of COMSOL Multiphysics. The elastic plate and the head-neck resonators were modeled using three-dimensional linear elasticity, without invoking any plate-wave

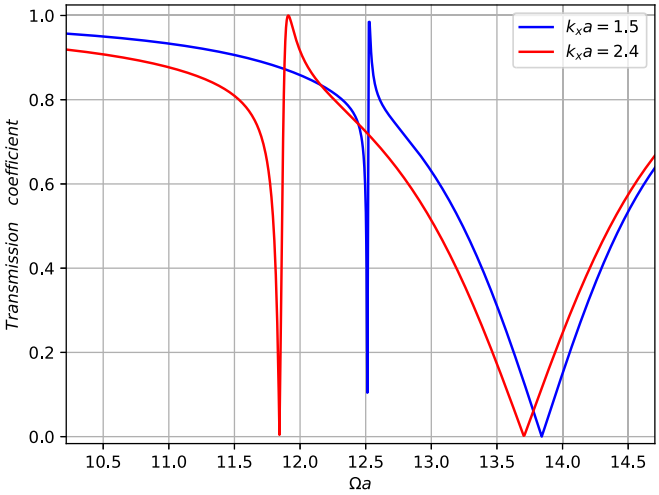

FIG. 7. Transmission coefficient as function of frequency for two different wave numbers $k_x a$ of the incident field.

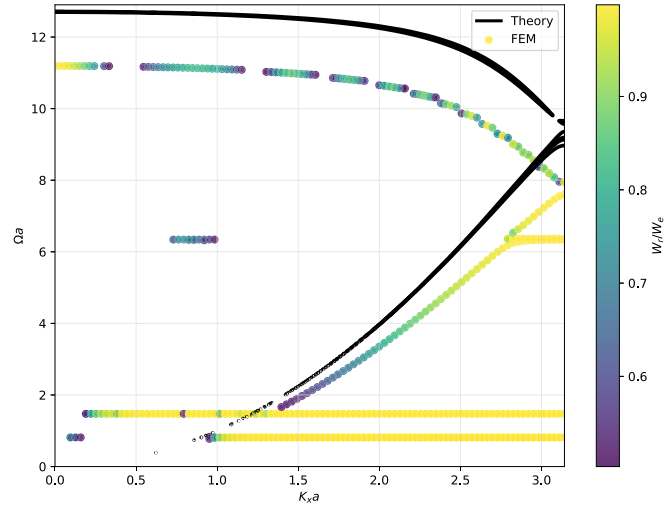

FIG. 8. Comparison between the dispersion relation obtained from the analytical pointlike resonator model (black lines) and from finite element method (FEM) simulations based on three-dimensional linear elasticity (colored symbols). The color scale represents an estimate of the mode quality factor, defined as the ratio between the elastic energy localized in the resonators and the total energy in the unit cell.

approximation. Periodic (Floquet-Bloch) boundary conditions were applied along the direction of periodicity.

For the calculation of the dispersion relation, periodic boundary conditions were also imposed in the directions perpendicular to the array, and the modes were identified by evaluating the elastic energy localized in the vicinity of the resonators. This procedure allows us to distinguish trapped and weakly radiative modes, and to estimate their quality factor by computing the ratio between the energy stored in the resonators and the total elastic energy within the unit cell.

For transmission and reflection calculations, perfectly matched layers (PMLs) were introduced in the transverse direction to suppress spurious reflections at the boundaries. A flexural plane wave was excited by imposing a uniform time-harmonic normal force on one side of the plate. The angle of incidence was controlled by rotating the excitation surface, thereby tuning the in-plane wave vector component k_x.

The geometrical parameters of the head-neck resonators were selected as $d_{\text{head}} = 0.32a$, $d_{\text{neck}} = 0.06a$, and $h_{\text{head}} = h_{\text{neck}} = 0.2a$. The resonators were assumed to be made of the same material as the plate (aluminum in this work), ensuring that the normalized mass γ and resonance frequency $\Omega_r a$ match those used in the analytical pointlike scattering model.

Figure 8 compares the dispersion relation obtained analytically using the pointlike resonator model (black lines) with that computed from FEM simulations (colored symbols). The color scale represents an estimate of the mode quality factor, obtained from the ratio between the elastic energy localized in the resonators (W_r) and the total energy in the unit cell (W_e). The agreement between both approaches is fair enough for the purposes of the current work at a qualitative and quantitative level: the QBIC branch is correctly reproduced, and the quality factor increases as the mode approaches the Γ point, while remaining high for modes below the radiation cone.

Some discrepancies between the two approaches are nevertheless observed. First, a global frequency shift appears, which is attributed to the approximate nature of the lumped head-neck model. Second, additional nearly flat modes emerge at lower frequencies in the FEM simulations, corresponding to internal bending resonances of the head-neck structures that are not captured by the Kirchhoff-Love plate approximation. Finally, small discontinuities in the QBIC branch are observed, which arise from hybridization with higher-order plate modes. Despite these differences, the essential physics of BIC and quasi-BIC formation is accurately described by the pointlike resonator model.

The excitation of quasi-BICs from the far field was also investigated using FEM simulations. The zeroth-order transmission coefficient T_0 was evaluated by computing the kinetic energy flux within a detection region located below the resonator array and normalizing it to the flux obtained in the absence of resonators:

$$T_0 = \frac{\iiint_S W_s \, dV}{\iiint_S W_0 \, dV}, \tag{19}$$

where W_s and W_0 denote the kinetic energy flux with and without the resonant structure, respectively, and S is the integration domain.

Figure 9 presents a direct comparison between the transmission spectra obtained from the analytical multiple-scattering model and the FEM simulations for two different incidence angles. A slight frequency shift is observed, primarily due to higher-order elastic effects and the finite spatial extent of the resonators, which are not included in the pointlike approximation. Nevertheless, the resonance positions, asymmetric Fano line shapes, and linewidths are remarkably well reproduced, confirming that the lumped head-neck model provides an accurate and efficient physical realization of the analytical system.

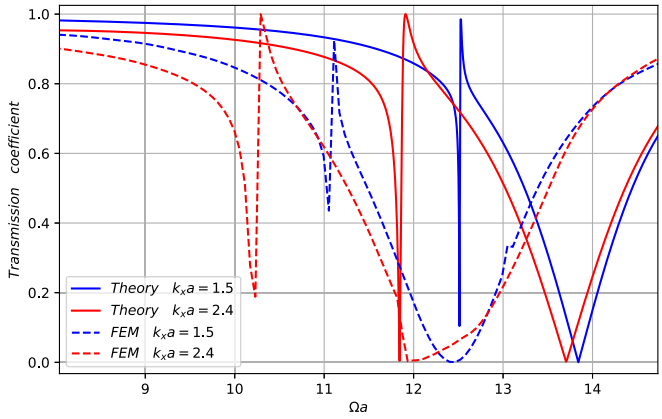

FIG. 9. Zeroth-order transmission coefficient as a function of frequency computed using the analytical multiple-scattering model (continuous lines) and FEM simulations (dashed lines) for two different incidence angles. The position, linewidth, and asymmetric Fano profiles of the quasi-BIC resonances are well reproduced by the analytical model, despite a small global frequency shift.

VI. SUMMARY

We have demonstrated that a simple one-dimensional array of dimerized resonators attached to a thin elastic plate supports both symmetry-protected BICs and tunable QBICs. At the Γ point, mirror symmetry enforces perfect confinement, while small geometric perturbations enable controllable far-field coupling with high quality factors. Away from Γ, finite Bloch momentum naturally breaks symmetry, giving rise to a dispersive QBIC band that can be excited at oblique incidence.

These results highlight the universality of BIC physics in elastic platforms and suggest practical opportunities for narrow band filtering, enhanced sensing, and nonlinear control of flexural waves. Future work will focus on experimental realization, refinement of the lumped resonator model, and theoretical extensions incorporating Rayleigh-wave contributions.

ACKNOWLEDGMENTS

We acknowledge Project No. CNS2023-145510 funded by MCIN/AEI/10.13039/501100011033, "European Union NextGenerationEU/PRTR", Project No. CIPROM/2023/44 funded by Generalitat Valenciana, and Project No. PID2024-158832NB-C22. This work was supported by DYNAMO project (101046489), funded by the European Union. Views and opinions expressed are however those of the authors only and do not necessarily reflect those of the European Union or European Innovation Council. Neither the European Union nor the granting authority can be held responsible for them.

DATA AVAILABILITY

No data were created or analyzed in this study.

[1] J. von Neumann and E. P. Wigner, Über merkwürdige diskrete eigenwerte, in *The Collected Works of Eugene Paul Wigner: Part A: The Scientific Papers*, edited by A. S. Wightman (Springer, Berlin, Heidelberg, 1993), pp. 291–293.

[2] F. H. Stillinger and D. R. Herrick, Bound states in the continuum, Phys. Rev. A **11**, 446 (1975).

[3] C. W. Hsu, B. Zhen, A. D. Stone, J. D. Joannopoulos, and M. Soljačić, Bound states in the continuum, Nat. Rev. Mater. **1**, 16048 (2016).

[4] J. Pappademos, U. Sukhatme, and A. Pagnamenta, Bound states in the continuum from supersymmetric quantum mechanics, Phys. Rev. A **48**, 3525 (1993).

[5] D. C. Marinica, A. G. Borisov, and S. V. Shabanov, Bound states in the continuum in photonics, Phys. Rev. Lett. **100**, 183902 (2008).

[6] Y. Yang, C. Peng, Y. Liang, Z. Li, and S. Noda, Analytical perspective for bound states in the continuum in photonic crystal slabs, Phys. Rev. Lett. **113**, 037401 (2014).

[7] K. Rong, *et al.*, Spin-valley Rashba monolayer laser, Nat. Mater. **22**, 1085 (2023).

[8] C. Schiattarella, S. Romano, L. Sirleto, V. Mocella, I. Rendina, V. Lanzio, and G. Zito, Directive giant upconversion by supercritical bound states in the continuum, Nature (London) **626**, 765 (2024).

[9] E. Melik-Gaykazyan, *et al.*, From Fano to quasi-BIC resonances in individual dielectric nanoantennas, Nano Lett. **21**, 1765 (2021).

[10] R. Ge, X. Liu, X. Yan, X. Chen, and Y. Chen, Doubly resonant photonic crystal cavity using merged bound states in the continuum, Phys. Rev. B **107**, 165406 (2023).

[11] A. F. Sadreev, Interference traps waves in an open system: bound states in the continuum, Rep. Prog. Phys. **84**, 055901 (2021).

[12] L. He, S. Sun, R. M. Abraham-Ekeroth, Y. Jin, Y. Xiang, and D. Torrent, Theoretical developments and experimental insights of acoustic and elastic bound states in the continuum, npj Acoustics **1**, 11 (2025).

[13] R. Parker, Resonance effects in wake shedding from parallel plates: Some experimental observations, J. Sound Vib. **4**, 62 (1966).

[14] R. Parker, Resonance effects in wake shedding from parallel plates: Calculation of resonant frequencies, J. Sound Vib. **5**, 330 (1967).

[15] Y. Plotnik, O. Peleg, F. Dreisow, M. Heinrich, S. Nolte, A. Szameit, and M. Segev, Experimental observation of optical bound states in the continuum, Phys. Rev. Lett. **107**, 183901 (2011).

[16] I. Deriy, I. Toftul, M. Petrov, and A. Bogdanov, Bound states in the continuum in compact acoustic resonators, Phys. Rev. Lett. **128**, 084301 (2022).

[17] B. Jia, L. Huang, A. S. Pilipchuk, S. Huang, C. Shen, A. F. Sadreev, and A. E. Miroshnichenko, Bound states in the continuum protected by reduced symmetry of three-dimensional open acoustic resonators, Phys. Rev. Appl. **19**, 054001 (2023).

[18] L. Huang, B. Jia, A. S. Pilipchuk, Y. Chiang, S. Huang, J. Li, C. Shen, E. N. Bulgakov, F. Deng, D. A. Powell, S. A. Cummer, Y. Li, A. F. Sadreev, and A. E. Miroshnichenko, General framework of bound states in the continuum in an open acoustic resonator, Phys. Rev. Appl. **18**, 054021 (2022).

[19] J. Fan, Z. Xue, H. Xing, D. Lu, G. Xu, J. Gu, J. Han, and L. Cong, Hybrid bound states in the continuum in terahertz metasurfaces, Opto-Electron. Sci. **2**, 230006 (2023).

[20] L. Nan, A. Mancini, T. Weber, G. L. Seah, E. Cortés, A. Tittl, and S. A. Maier, Angular dispersion suppression in deeply subwavelength phonon polariton bound states in the continuum metasurfaces, Nat. Photon. **19**, 615 (2025).

[21] Z. Wen, P. Gao, J. Mao, S. Dai, M. Marti-Sabaté, Y. Jin, D. Torrent, and Y. Qu, Compact metaplate with bound state in the continuum: From quasisymmetry to symmetry, Phys. Rev. Lett. **135**, 087201 (2025).

[22] Y. Jin, E. H. E. Boudouti, Y. Pennec, and B. Djafari-Rouhani, Tunable Fano resonances of lamb modes in a pillared metasurface, J. Phys. D **50**, 425304 (2017).

[23] W. Wang, Y. Jin, W. Wang, B. Bonello, B. Djafari-Rouhani, and R. Fleury, Robust Fano resonance in a topological mechanical beam, Phys. Rev. B **101**, 024101 (2020).

[24] G. Sun, Y. Wang, Y. Li, Z. Cui, W. Chen, and K. Zhang, Tailoring topological nature of merging bound states in the continuum by manipulating structure symmetry of the all-dielectric metasurface, Phys. Rev. B **109**, 035406 (2024).

[25] K. Koshelev, S. Lepeshov, M. Liu, A. Bogdanov, and Y. Kivshar, Asymmetric metasurfaces with high-Q resonances governed by bound states in the continuum, Phys. Rev. Lett. **121**, 193903 (2018).

[26] L. Kühner, L. Sortino, R. Berté, J. Wang, H. Ren, S. A. Maier, and A. Tittl, Radial bound states in the continuum for polarization-invariant nanophotonics, Nat. Commun. **13**, 4992 (2022).

[27] C. W. Hsu, B. Zhen, S. L. Chua, S. G. Johnson, J. D. Joannopoulos, and M. Soljačić, Bloch surface eigenstates within the radiation continuum, Light Sci. Appl. **2**, e84 (2013).

[28] D. Torrent, D. Mayou, and J. Sánchez-Dehesa, Elastic analog of graphene: Dirac cones and edge states for flexural waves in thin plates, Phys. Rev. B **87**, 115143 (2013).

[29] Y. Jin, D. Torrent, and B. Djafari-Rouhani, Robustness of conventional and topologically protected edge states in phononic crystal plates, Phys. Rev. B **98**, 054307 (2018).

[30] M. Martí-Sabaté and D. Torrent, Edge modes for flexural waves in quasi-periodic linear arrays of scatterers, APL Mater. **9**, 081107 (2021).

[31] M. Martí-Sabaté, J. Li, B. Djafari-Rouhani, S. A. Cummer, and D. Torrent, Observation of two-dimensional acoustic bound states in the continuum, Commun. Phys. **6**, 198 (2023).

[32] A. Colombi, D. Colquitt, P. Roux, S. Guenneau, and R. V. Craster, A seismic metamaterial: The resonant metawedge, Sci. Rep. **6**, 27717 (2016).

[33] V. Laude, Complex dispersion relation of Rayleigh-Bloch waves trapped by slow inclusions, Phys. Rev. B **111**, L220101 (2025).

[34] L. G. Bennetts and M. A. Peter, Rayleigh–Bloch waves above the cutoff, J. Fluid Mech. **940**, A35 (2022).

[35] G. J. Chaplain, S. C. Hawkins, M. A. Peter, L. G. Bennetts, and T. A. Starkey, Acoustic lattice resonances and generalised Rayleigh-Bloch waves, Commun. Phys. **8**, 37 (2025).

[36] R. Chaunsali, C.-W. Chen, and J. Yang, Subwavelength and directional control of flexural waves in zone-folding induced topological plates, Phys. Rev. B **97**, 054307 (2018).

[37] P. Packo, A. N. Norris, and D. Torrent, Inverse grating problem: Efficient design of anomalous flexural wave reflectors and refractors, Phys. Rev. Appl. **11**, 014023 (2019).

[38] K. F. Graff, *Wave Motion in Elastic Solids* (Courier Corporation, North Chelmsford, MA, 2012).

[39] M. Martí-Sabaté, S. Guenneau, and D. Torrent, High-quality resonances in quasi-periodic clusters of scatterers for flexural waves, AIP Adv. **12**, 085303 (2022).